NEW RESULTS ON DIMUON PRODUCTION BY HIGH ENERGY NEUTRINOS AND ANTINEUTRINOS

T.Y. Ling
Department of Physics
The Ohio State University
Columbus, Ohio 43210
USA

I. Introduction

The subject of multimuon production by high energy neutrinos and anti-neutrinos began more than three years ago with the observation of dimuons by the HPWF collaboration at Fermilab.[1] The opposite sign dimuon events were interpreted as evidence for a new hadronic quantum number - charm.[2,3] Much has been learned since then. Recent experiments[4] not only confirmed the earlier observation but also supported the 'charm' interpretation. The origin of the like-sign dimuons ($\mu^-\mu^-$) remain, however, unknown. Because of the smaller observed rate for these events, decays of pions and kaons from ordinary deep inelastic neutrino interactions might account for a large fraction, if not all, of the observed events. It is important to determine whether 'prompt' like-sign dimuons exist, for the rate and nature of the prompt $\mu^-\mu^-$ events would provide important clues to the overall understanding of another facet of multimuon phenomena, in particular, the recently discovered trimuon events.[5]

In this talk I would like to report on recent dimuon data from the FHOPRW collaboration (E-310) at Fermilab. The issues I will concentrate on are: Is there a prompt like-sign dimuon signal? What are the nature of these like-sign events as compared to the opposite sign events? How consistent are the rates and properties of the opposite sign events with charm particle production and their semi-leptonic decay? The trimuon events observed during the same runs from which the present dimuon samples were obtained have already been published and reported at various other conferences and therefore will not be discussed here.

II. Beams

The data samples reported here were acquired at Fermilab in three runs, using a quadrupole triplet (QT) and sign-selected bare target (SSBT) beams. In the QT beam the secondary hadrons produced in the proton-target collision were focussed by a quadrupole triplet and left to decay without charge selection.[6] The resultant neutrino flux contains a mixture of ν_μ and $\bar{\nu}_\mu$. The SSBT beams employed no focussing elements but did charge selection of the secondary hadrons by means of a "dog-leg" arrangement of bending magnets.[7] Hence the resultant beams contain only ν_μ or $\bar{\nu}_\mu$ depending on the selected sign of the parent hadrons. These will be referred to as the SSBTν and SSBT$\bar{\nu}$ beams. The calculated spectra of ν_μ and $\bar{\nu}_\mu$ from these beams are shown in Fig. 1. The QT and SSBTν runs yielded 199 $\mu^-\mu^+$ events and 46 $\mu^-\mu^-$ events. The SSBT$\bar{\nu}$ run yielded 49 $\mu^+\mu^-$ events and 2 $\mu^+\mu^+$ events.

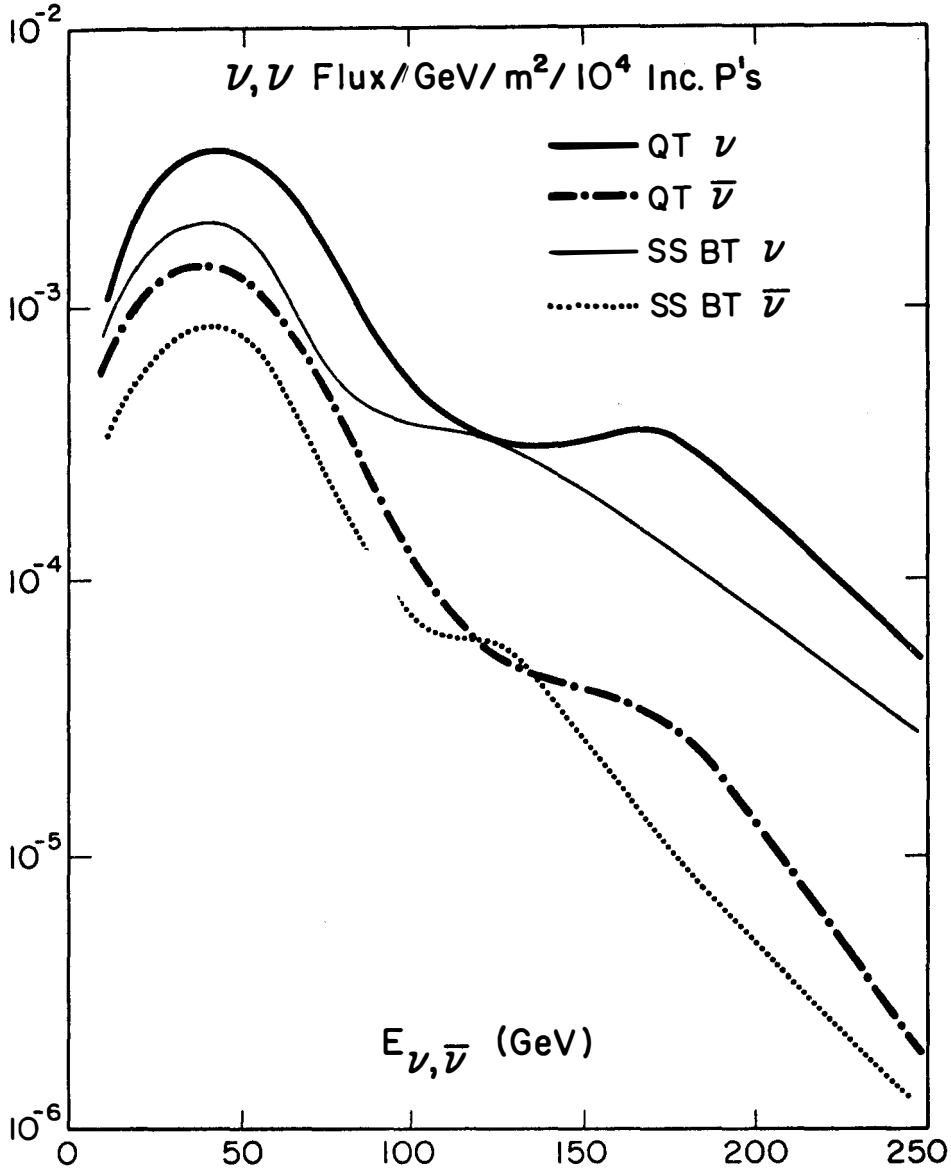

Fig. 1 Calculated neutrino and antineutrino spectra for the Quadrupole Triplet and Bare Target Selected Beams.

III. Detector

The detector of E-310 is shown in Fig. 2. It is an enlarged version of the earlier detector of E-1A with important modifications. i) A target-detector of three parts, an iron target (FeT), a liquid scintillator calorimeter (LiqC), and an iron-plate (4" thick plates) calorimeter (FeC), each part of different density. This makes possible an empirical determination of the pion and kaon decay background in the multimuon data. Table I shows the hadronic absorption length and fiducial masses of the three target-detectors. ii) A large solid angle muon spectrometer consists of three large area toroidal magnets (24' diameter) in addition to the existing 12' diameter toroids. Muons of angles up to 500 mrad relative to the ν_μ beam direction can be detected, compared with the limited angle of 225 mrad of E1A.

IV. Like-Sign Dimuons

1. Existence of a Prompt Signal?

The issue of foremost importance is to determine whether the like-sign dimuons are indeed all due to pion and kaon decays. This can in principle be inferred from the observed $\mu^-\mu^-$ rate produced in each target. The relative rates $R(\mu^-\mu^-)/R(\mu^-)$ are difficult to determine because of differences in acceptance, trigger requirements, etc between the targets. The ratio $N(\mu^-\mu^-)/N(\mu^-\mu^+)$ is, however, insensitive to these target dependent systematic effects, for to a good approximation these are the same for both the $\mu^-\mu^+$ and $\mu^-\mu^-$ events. The numbers of observed $\mu^-\mu^+$ and $\mu^-\mu^-$ events are shown in columns 3 and 5 of Table I for muon momentum cuts p>5 and 10 Gev/c respectively. The ratios $N^{obs}(\mu^-\mu^+)/N^{obs}(\mu^-\mu^+)$ are plotted against absorption length in Figs. 3a and 3b. To simplify the interpretation, we subtract from $N^{obs}(\mu^-\mu^+)$ the calculated numbers of the $\mu^-\mu^+$ events resulting from π and K decays[8], also listed in Table 1. The numbers of prompt $\mu^-\mu^+$ events are then given by $N^{obs}(\mu^-\mu^+)-N^{decay}(\mu^-\mu^+)$. In Figs. 3c and 3d, we show the ratios $N^{obs}(\mu^-\mu^-)/N^{prompt}(\mu^-\mu^+)$, again for the muon momentum cuts p>5 and 10 Gev/c. Linear fits to the data with both the slope and intercept as free parameters, are also shown. We observe that i) the decay of pions and kaons account for a significant fraction of the $\mu^-\mu^-$ events for the case $p_\mu > 5$ Gev/c; ii) the fitted slope decreases as the minimum momentum cut of the muon is raised from 5 to 10 Gev/c, resulting from the reduction of pion and kaon decay backgrounds as expected, and iii) the intercept of the fits at zero absorption length (infinite density) are different from zero in both cases.

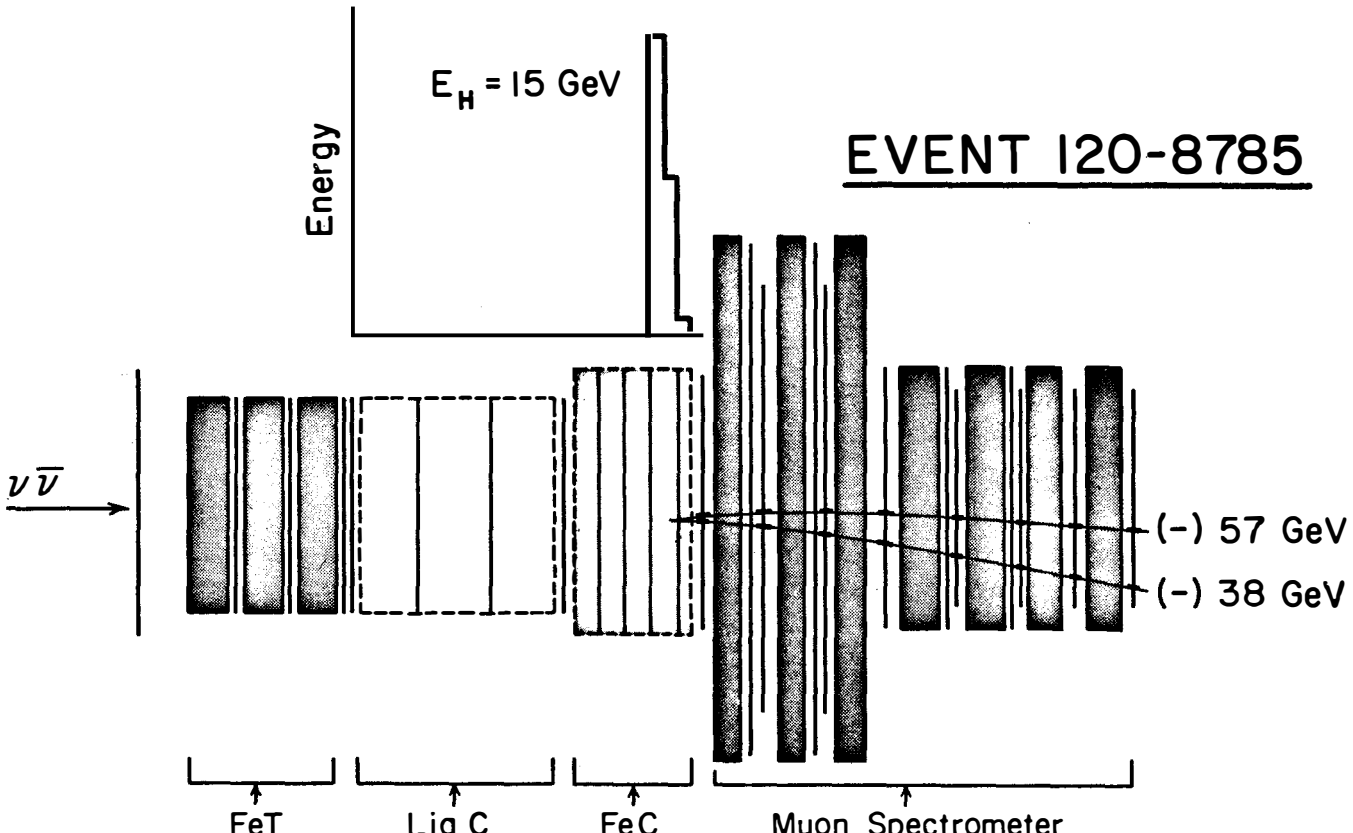

Fig. 2 Schematic layout of the E-310 Neutrino Detector. The tracing of an observed $\mu^-\mu^-$ event is superimposed on the apparatus.

TARGET	FIDUCIAL MASS (Tons)	ABS. LENGTH (cm)	$N^{obs}(\mu^-\mu^+)$		$N^{decay}(\mu^-\mu^+)$		$N^{obs}(\mu^-\mu^-)$		$N^{decay}(\mu^-\mu^-)$	
			$p_\mu>5$ GeV	$p_\mu>10$ GeV	$p_\mu>5$ GeV	$p_\mu>10$ GeV	$p_\mu>5$ GeV	$p_\mu>10$ GeV	$p_\mu>5$ GeV	$p_\mu>10$ GeV
IRON (FeT)	198	31	75	50	11	3.5	12	8	6.1	1.6
IRON CAL. (FeC)	42	61	42	23	10.5	2.6	10	4	5.9	1.5
LIQ. CAL. (LiqC)	36	120	56	32	22.2	7.7	16	6	12.0	3.2
TOTAL			173	105	43.7	13.8	38	18	24.0	6.3

TABLE 1. Fiducial masses, absorption lengths and numbers of observed dimuon events in the three targets. Also shown are the calculated numbers of dimuon events from pion and kaon decays.

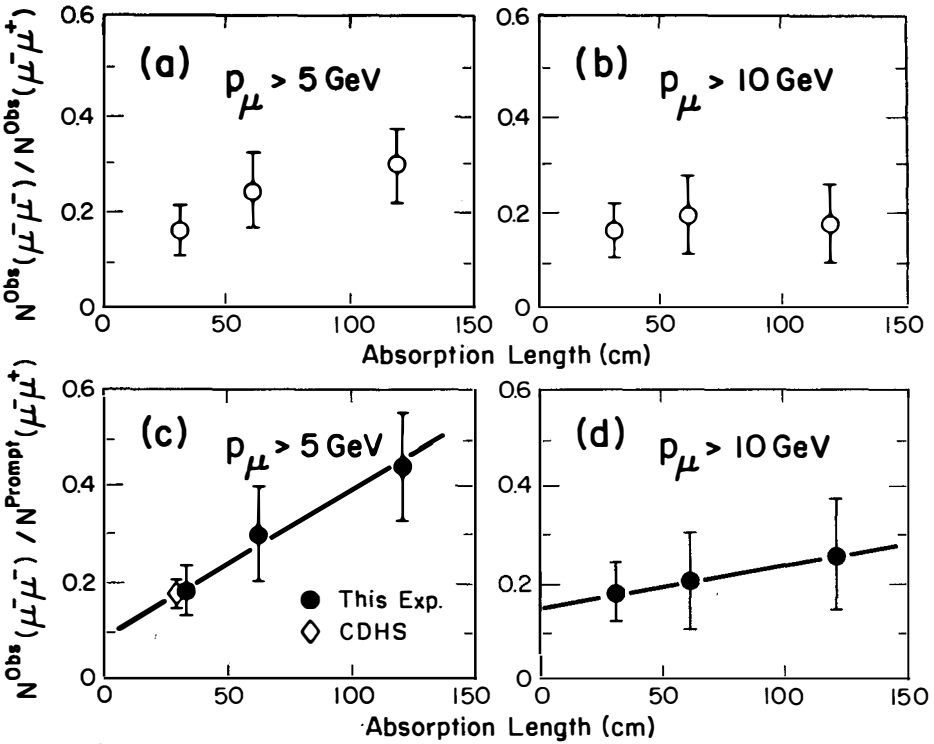

Fig. 3 Ratios of observed numbers of $\mu^-\mu^-$ events to that of the $\mu^-\mu^+$ events against hadronic absorption length for (a) p_μ > 5 Gev and (b) p_μ > 10 Gev. Ratios of observed numbers of $\mu^-\mu^-$ events to the $\frac{\text{prompt}}{p_\mu > 5}$ $\mu^-\mu^+$ events against hadronic absorption length for (c) Gev and (d) p_μ > 10 Gev.

It should be noted that although the analysis described above depend to some extent on the correction to subtract π, K decay contribution from $N^{obs}(\mu^-\mu^+)$, the value of the intercept from the extrapolation is relatively insensitive to this correction. The reason for this is that π and K decay contributions are relatively much smaller fraction of the $\mu^-\mu^+$ events. This is true especially for the FeT point which carries a lot of weight in determining the value of the intercept. Nonetheless, we have checked the reliability of the π, K decay calculation by comparing the density dependence of $N^{obs}(\mu^-\mu^+)/N(\mu^-)$. This comparision is shown in Fig. 4. The calculated slope is found to be very consistent with the data as shown. We further note that the fitted slope for the $p_\mu > 5$ Gev/c data in Fig. 3c is $(3.0 \pm 1.0)\times10^{-3}cm^{-1}$, also in good agreement with the value $(2.7 \pm 0.7)\times10^{-3}cm^{-1}$ obtained from the calculated numbers $N^{decay}(\mu^-\mu^-)$ shown in Table 1. These agreements check the validity of the decay calculation and gives us confidence in using the calculated numbers $N^{decay}(\mu^-\mu^-)$ to determine the magnitude of the prompt $\mu^-\mu^-$ signal in each target. The result is shown in Fig. 5. The ratios $N^{prompt}(\mu^-\mu^-)/N^{prompt}(\mu^-\mu^+)$ are seen to be systematically non-zero and independent of absorption length. Averaging over all three targets we obtain $N^{prompt}(\mu^-\mu^-)/N^{prompt}(\mu^-\mu^+) = 0.10 \pm 0.05$ for $p_\mu > 5$ Gev/c, and 0.13 ± 0.05 for $p_\mu > 10$ Gev/c.

In a run using the dichromatic beam at CERN, the CDHS collaboration reported the observation of 257 $\mu^-\mu^+$ events and 47 $\mu^-\mu^-$ events which satisfy the muon momentum cutoff of 4.5 Gev/c.[9] The ratio $N^{obs}(\mu^-\mu^-)/N^{prompt}(\mu^-\mu^+)$ for $p_\mu > 5$ Gev, obtained using the reported[9] π, K decay contributions and the slow muon momentum spectra, is 0.17 ± 0.03. The target detector of the CDHS experiment is primarily iron with an average hadronic absorption length of 30 cm. The CDHS result is plotted on Fig. 3c for comparison with this experiment. The good agreement between the two experiments supports our measurement in the iron target.

The two $\mu^+\mu^+$ events observed in the SSBT($\bar{\nu}$) run have very low energy muons ($\approx$5 Gev/c). Pion and kaon decays are estimated to yield 4 ± 2 events. Hence the two observed events are consistent with being backgrounds. If a prompt $\mu^+\mu^+$ signal were to exist at the same rate relative to the $\mu^+\mu^-$ event as the $\mu^-\mu^-$ signal, we would expect to observe 5 events in addition. So from this sample there is as yet no clear evidence of a prompt $\mu^+\mu^+$ signal.

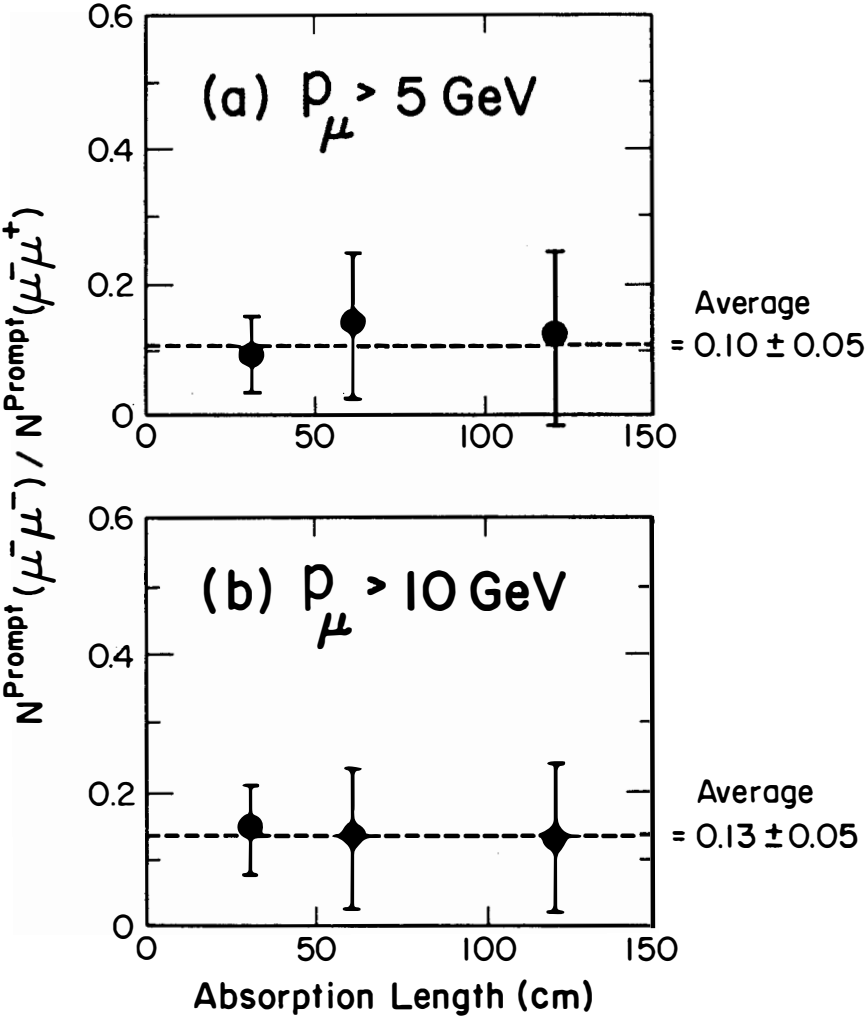

Fig. 4 Number of prompt $\mu^-\mu^-$events in each of the three targets for (a) $p_\mu > 5$ Gev and (b) $p_\mu > 10$ Gev.

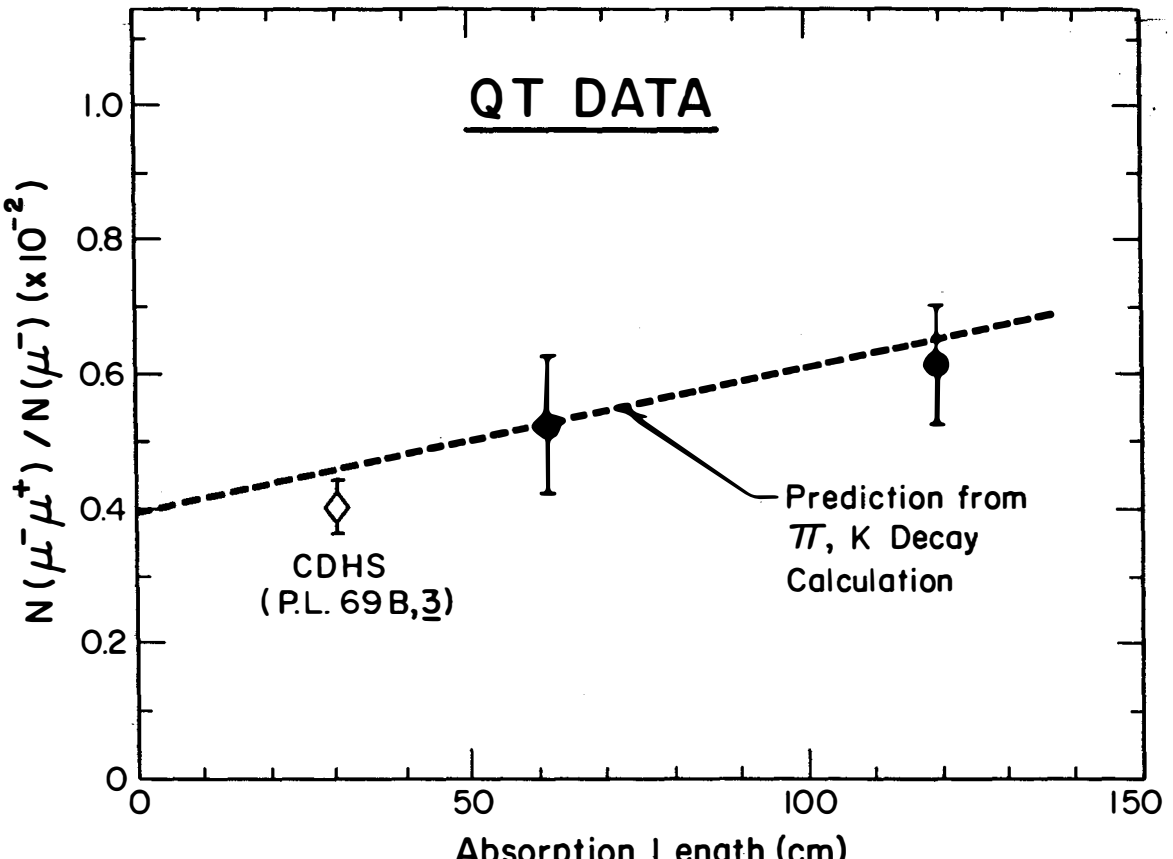

Fig. 5 Numbers of opposite sign dimuon events relative to that of the single muon events vs of hadronic absorption length.

2. Properties of the $\mu^-\mu^-$ events

The important properties of the $\mu^-\mu^-$ events are shown in Figures 6 - 10. Figure 6 shows the scatter plot of the momentum of the fast μ^- against the slow μ^-. A rather large momentum asymmetry between the two muons is observed, similar to that observed in the $\mu^-\mu^+$ data as shown in Fig. 7. The distribution in the azimuthal angle between the two muons is shown in Fig. 8a and 8b for the $\mu^-\mu^-$ and $\mu^-\mu^+$ events. Both distributions tend to peak at $\Delta\Phi = 180^\circ$, suggestive of a hadronic origin for the second muon. Fig. 9a shows the distribution in $p^s_{\perp W}$, the transverse momentum of the slow μ^- with respect to the direction of the W-boson which is defined by the directions of the incident neutrino and the fast μ^-. Again for comparison we show in Fig. 9 the distribution in $p^+_{\perp W}$ of the μ^+ for the $\mu^-\mu^+$ events. No distinctive differences can be seen. The distribution in the E_{vis} distributions are also similar between the $\mu^-\mu^-$ and $\mu^-\mu^+$ events as shown in Fig. 10a and 10b.

It could be argued that since a significant fraction of the $\mu^-\mu^-$ events are in fact from π or K decays, the properties of the prompt events could be largely masked. For this reason, the $\mu^-\mu^-$ events which satisfy the 10 Gev momentum cut are shaded for comparison. Contamination of pion and kaon decays are much smaller in this case. We note that although the statistics is very limited, the distribution exhibit the same general features. Properties of energetic $\mu^-\mu^-$ events where both muons have $p_\mu > 15$ Gev are shown in Table 2.

V. Opposite-Sign Dimuons

We now turn to the measurements of the rates of opposite-sign dimuons. The observed E_{vis} ($\equiv E_h + E_{\mu^-} + E_{\mu^+}$) distribution for the $\mu^-\mu^+$ events from the QT run is shown in Fig. 11a. The energy spectrum of the single muon events from the same run is shown in Fig. 11b. Figure 11 shows the relative rate $R(\mu^-\mu^+)/R(\mu^-)$ as a function of $E_{\ }$. Two things were further taken into account to obtain the data points shown in Fig. 13. First, the dimuon events were individually weighted by a factor which corrected for the geometric acceptance and triggering biases. This weighting factor was calculated for each of the observed events by azimuthally rotating the event in the detector. Secondly, the contribution from π and K decays had been subtracted from the data. Figs. 12 and 14 show the corresponding data for $\bar{\nu}$ induced $\mu^+\mu^-$ events from the SSBT($\bar{\nu}$) run. We note that the apparent rise in the dimuon rate relative to single muon rate with energy for both the ν and $\bar{\nu}$ samples are predominantly the result of the 5 Gev/c momentum cut.

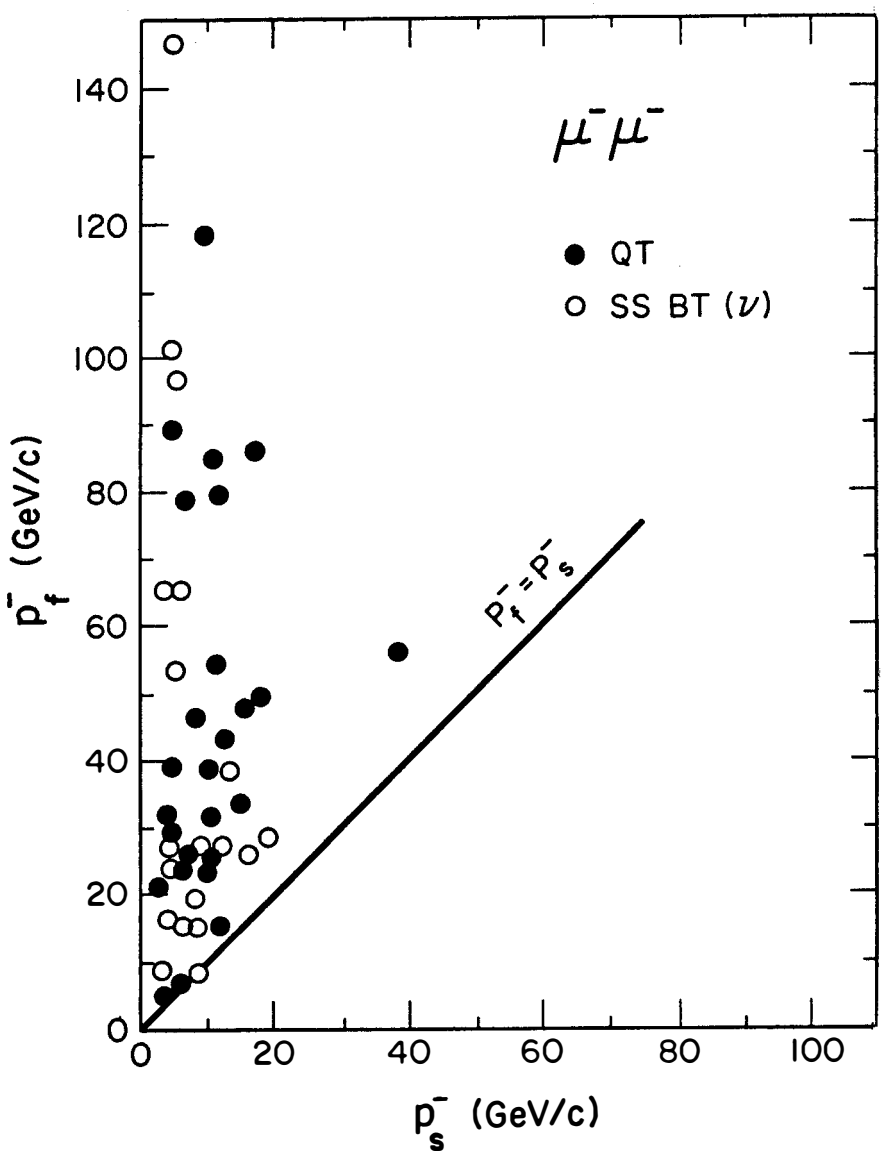

Fig. 6 Scatter plot of the muon momenta for the like-sign dimuon events.

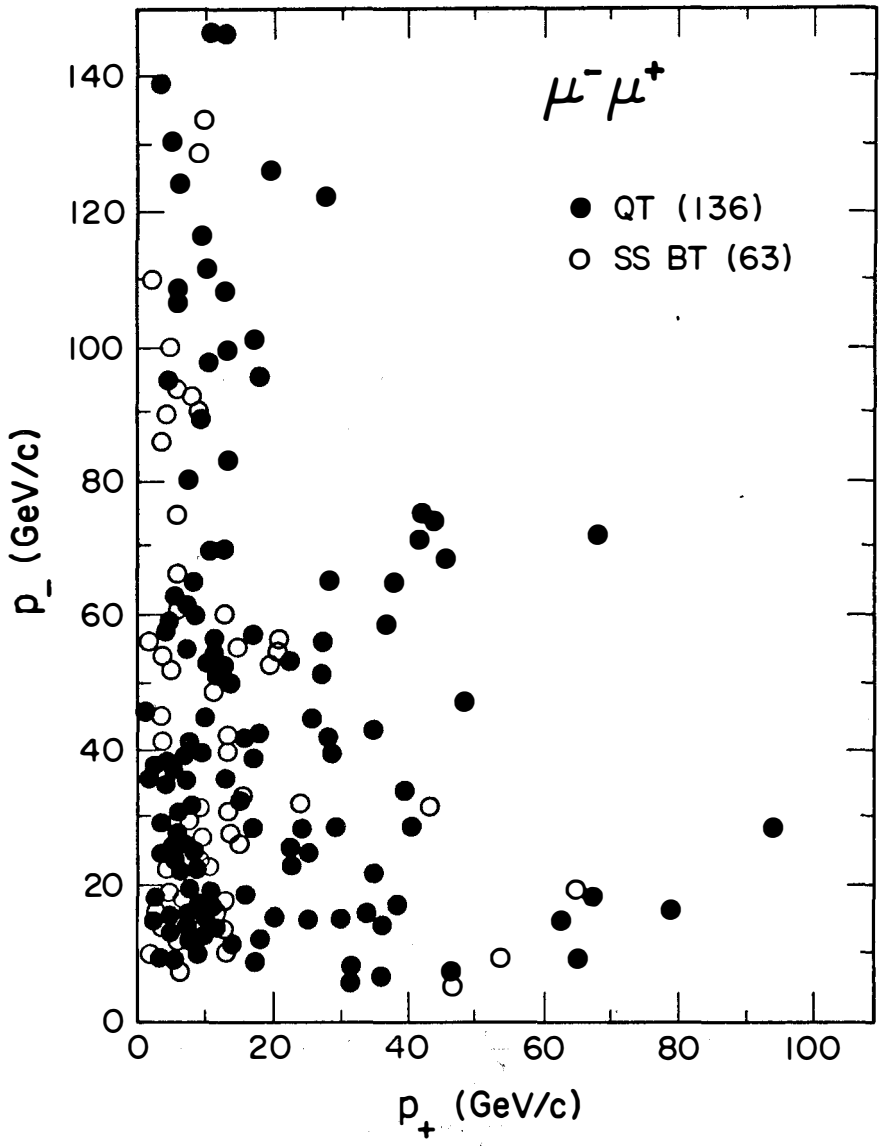

Fig. 7 Scatter plot of the muon momenta for the opposite sign dimuon events.

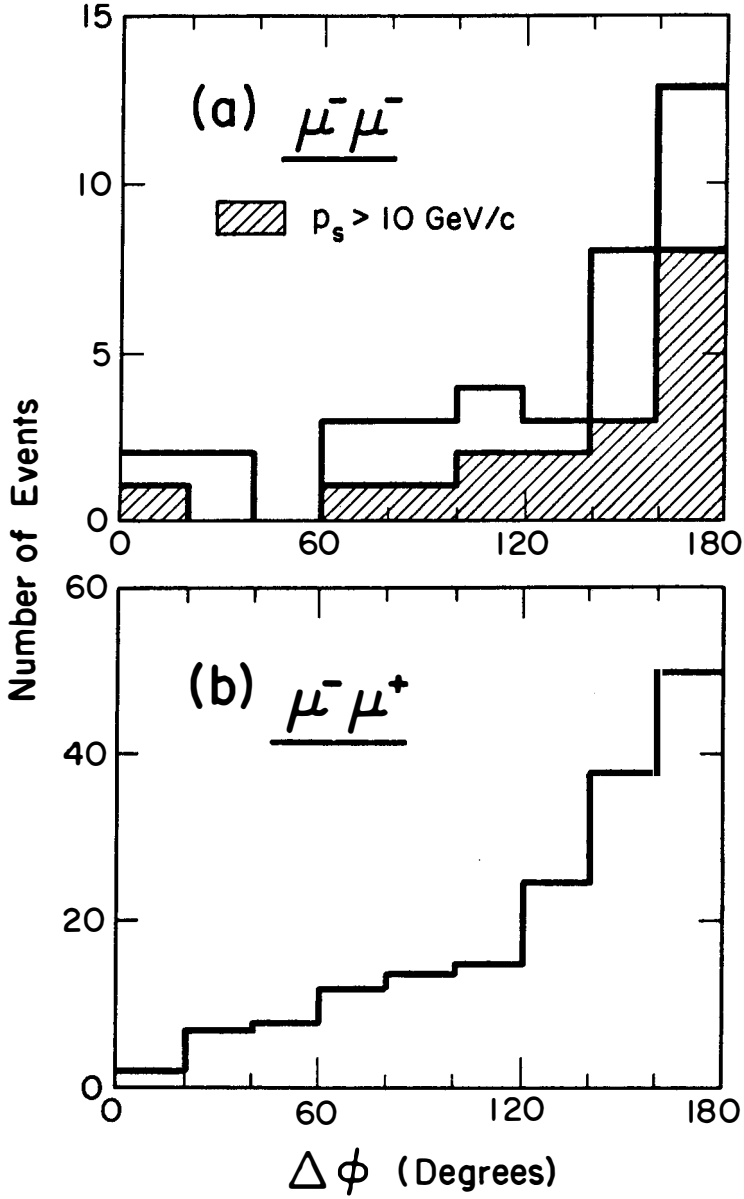

Fig. 8 Distributions in the relative azimutha angle, $\Delta\phi$ between the two muons for (a) the like-sign dimuons and (b) the opposite-sign dimuons.

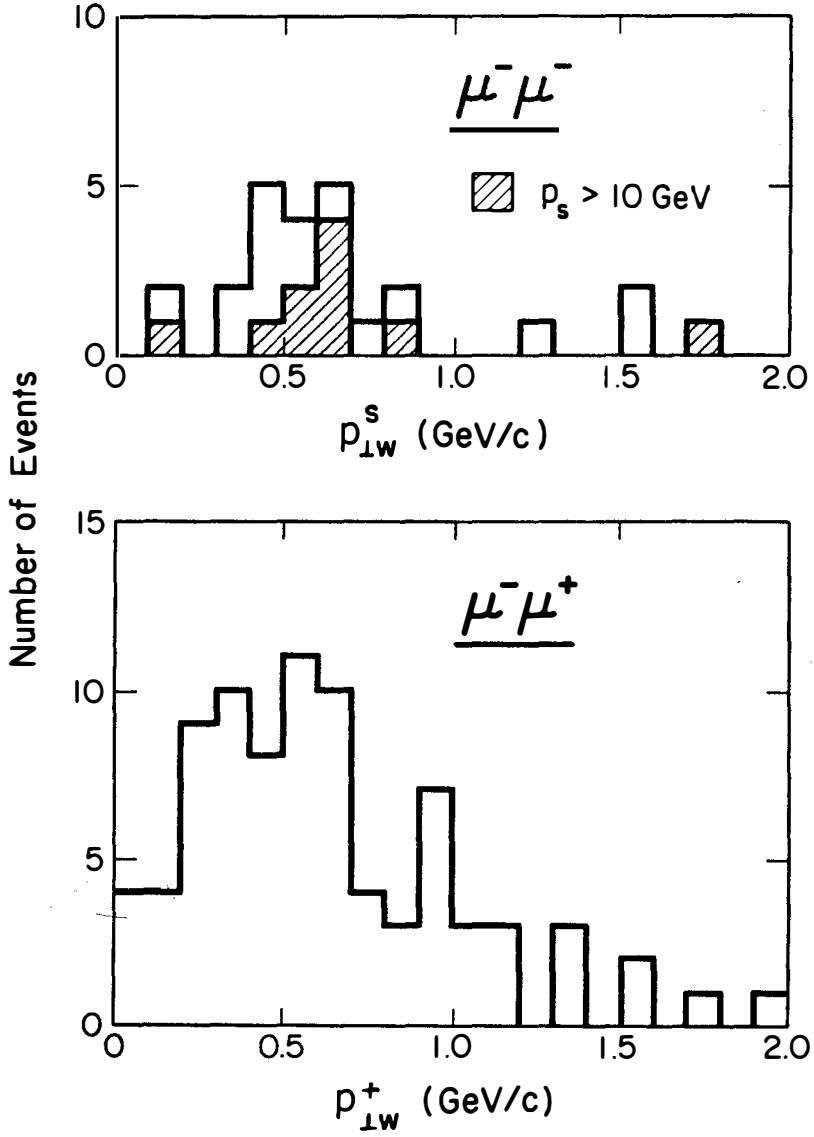

Fig. 9 Distributions in the transverse momentum relative to the W-direction for the (a) like-sign dimuons and (b) opposite-sign dimuons.

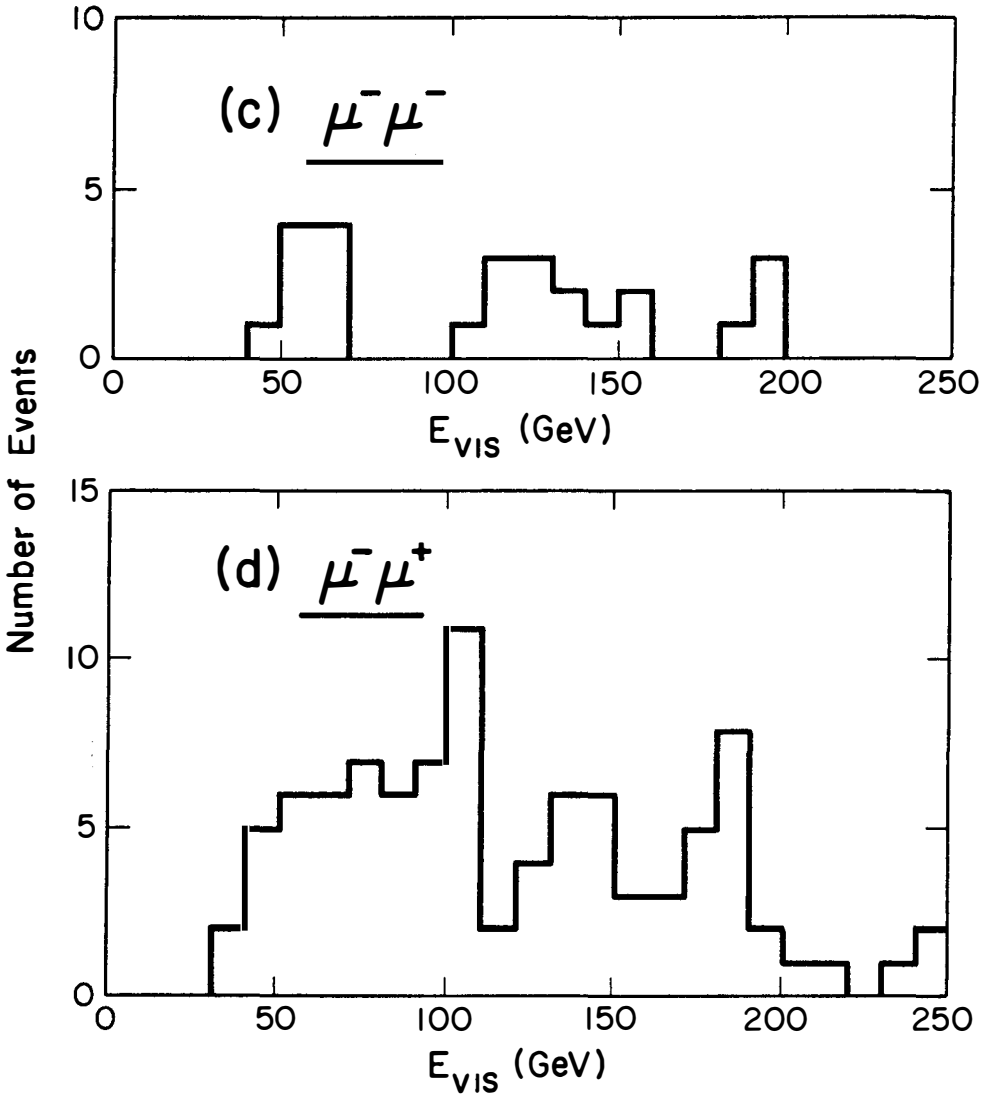

Fig.10 Distributions of total visibleenergy for (a) like-sign dimuons and (b) opposite-sign dimuons.

RUN FRAME	TGT MOD	ENERGY (GeV)		TRACK 1			TRACK 2		
		E_{vis}	E_h	QP	Px	Py	QP	Px	Py
117 15365	Liq 13	127	24	-86 ±7.3	1.87 ±.13	.21 ±.04	-17 ±.7	-1.42 ±.06	.07 ±.05
120 18783	FeC 21	114	19	-57 ±5.7	.27 ±.13	-1.22 ±.23	-38 ±4.4	.52 ±.17	1.21 ±.11
137 31940	FeT 2	>110	>46	-48 ±3.2	.50 ±.04	1.05 ±.11	-16 ±1.2	-.23 ±.08	.27 ±.09
141 35757	FeT 1	> 48	-	-33 ±12.8	.87 ±.23	-2.02 ±.65	-15 ±1.2	-.35 ±.14	.71 .05
146 39767	FeT 2	> 67	-	-49 ±3.8	1.94 ±.11	-.09 ±.06	-18 ±1.5	-.82 ±.06	.15 ±.06
279 145416	FeC 20	12	83	-26 ±2.2	-.69 ±.12	1.34 ±.13	-16 ±1.3	.52 ±.05	-.59 ±.05
282 149196	FeT 3	>58	>11	-28 ±1.4	.96 ±.05	-1.33 ±.04	-19 ±1.1	-.83 ±.04	.15 ±.04

TABLE 2. Properties of the energetic $\mu^-\mu^-$ events ($p_\mu > 15$ GeV).

Units of all momenta are in GeV.

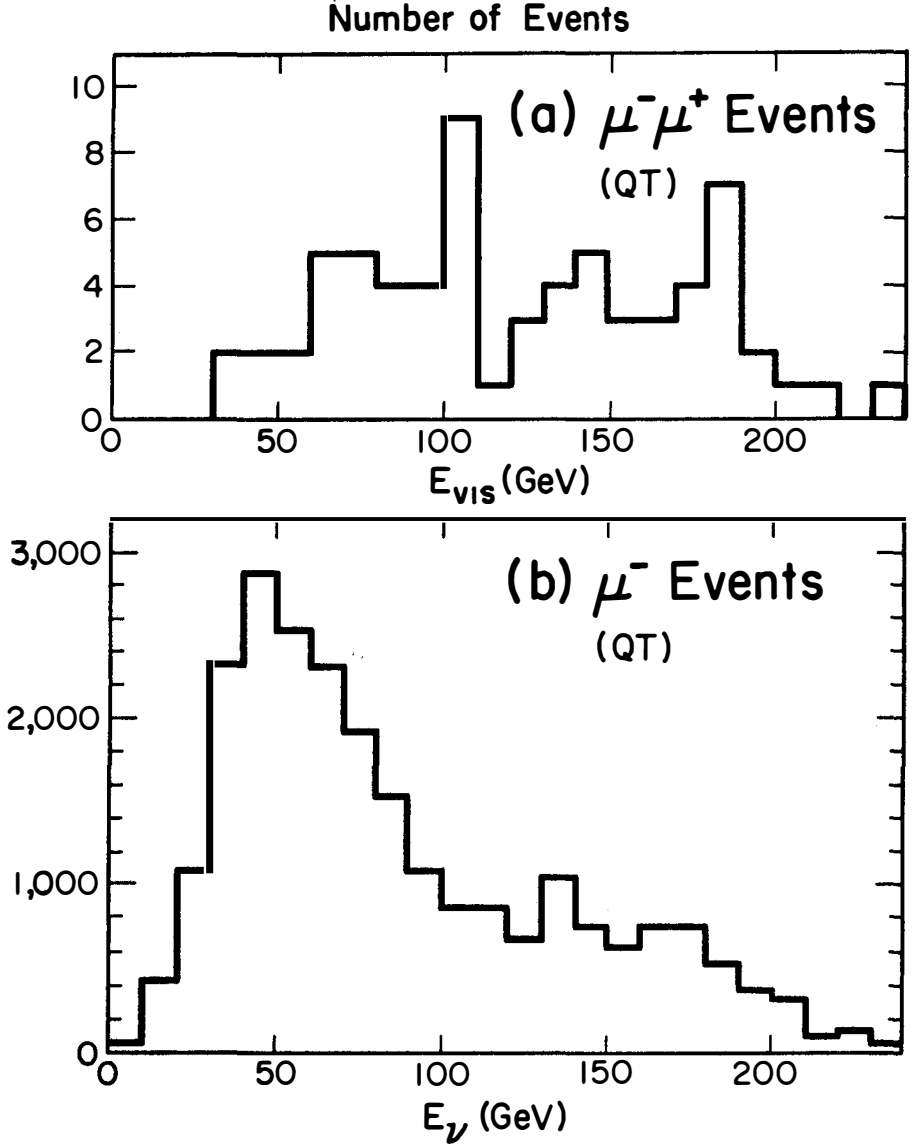

Fig.11 (a) Distributions of total visible energy for the ν-induced opposite-sign dimuons, (b) Distributions of neutrino energy for the ν-induced single muon events.

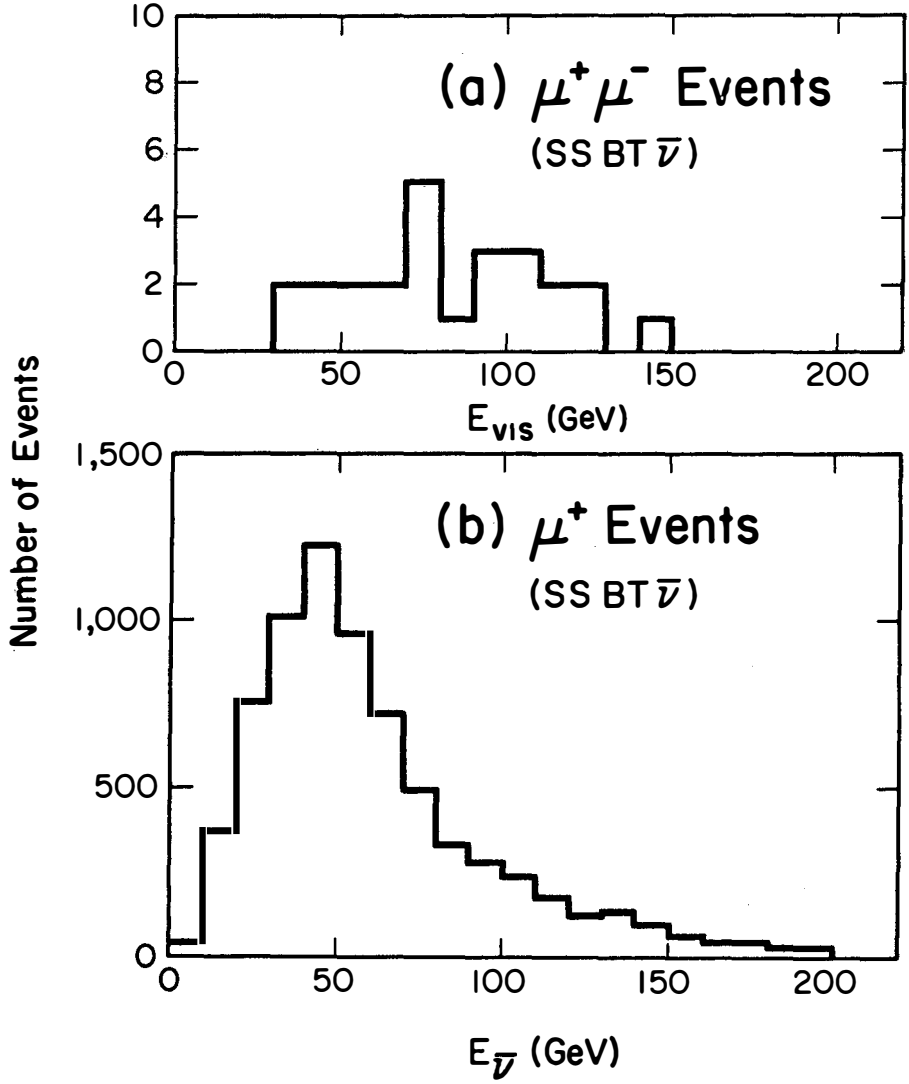

Fig.12 (a) Distributions of total visible energy for the $\bar{\nu}$-induced opposite-sign dimuons events, and (b) distributions of antineutrino energy for the $\bar{\nu}$-induced single muon events.

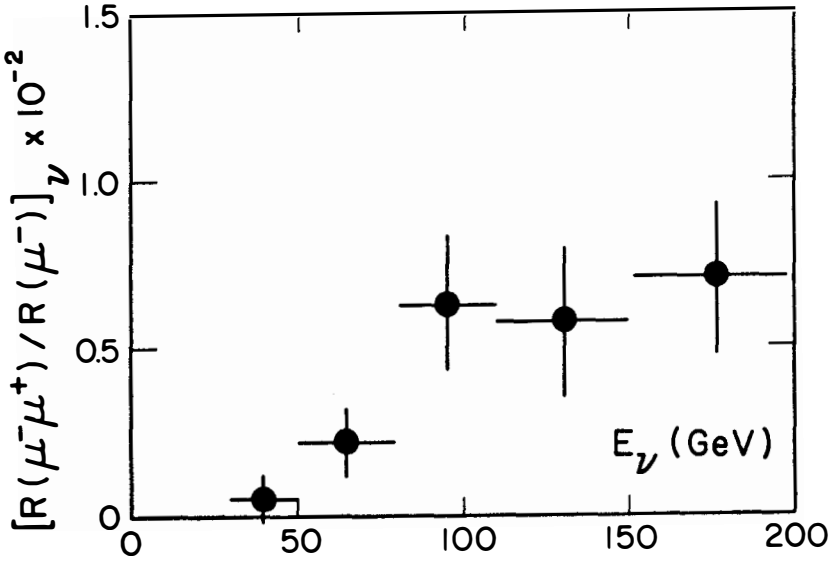

Fig.13 Rate of $\mu^-\mu^+$ events relative to rate of single muon events as a function of energy for neutrinos.

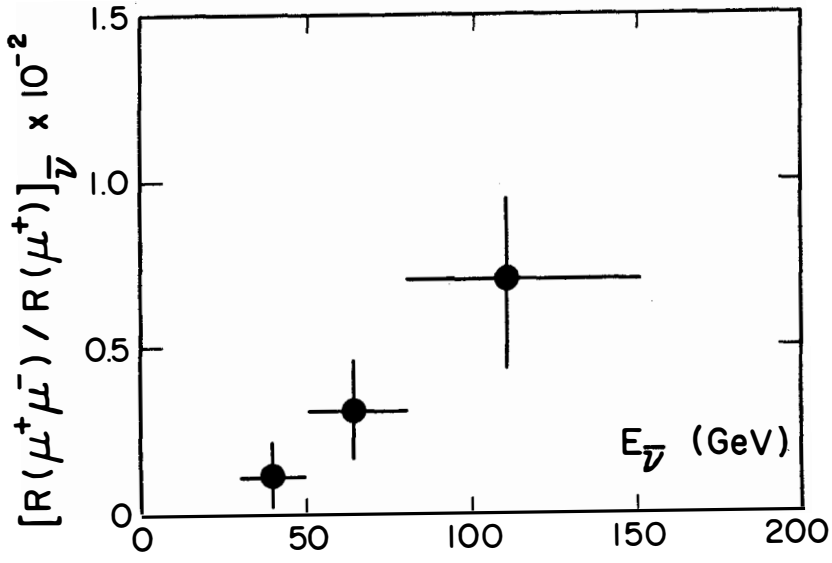

Fig.14 Rate of $\mu^-\mu^+$ events relative to rate of single muon events as a function of energy for antineutrinos.

The relative rates averaged over the corresponding beam energy spectra are

$$\{R(\mu^-\mu^+)/R(\mu^-)\}\quad \nu(30\text{-}200\ \text{Gev}) = (0.4 \pm 0.08) \times 10^{-2}$$

and

$$\{R(\mu^-\mu^+)/R(\mu^+)\}\quad \bar{\nu}(30\text{-}200\ \text{Gev}) = (0.27 \pm 0.09) \times 10^{-2}$$

The average $\bar{\nu}$ dimuon rate is lower because the SSBT($\bar{\nu}$) spectrum is substantially softer than the QT neutrino spectrum. For a given energy bin, we observe that the $\mu^-\mu^+$ rate relative to single μ rate is approximately the same for the ν and $\bar{\nu}$ data. At high energy, say $E_{vis} > 80$ Gev, where acceptance due to kinematic cutoff is less limited we have

$$\{R(\mu^-\mu^+)/R(\mu^-)\}\quad \nu(>80\ \text{Gev}) = (0.65 \pm 0.13) \times 10^{-2}$$

and

$$\{R(\mu^-\mu^+)/R(\mu^+)\}\quad \bar{\nu}(>80\ \text{Gev}) = (0.70 \pm 0.25) \times 10^{-2}$$

If we assume $\sigma^{\bar{\nu}}/\sigma^{\nu} \simeq 0.5$, it then follows from the data that

$$R^{\nu}(\mu^-\mu^+)/R^{\bar{\nu}}(\mu^+\mu^-) \simeq 2.$$

To compare this with the prediction of the GIM model, we note that in that model, charm quarks are produced by neutrino through their interaction either with the d(valence) or with the s(sea) quarks, namely,

$$\nu + d \to \mu^- + c\ ;\ (\sigma \propto \sin^2\theta_c)$$

$$\nu + s \to \mu^- + c\ ;\ (\sigma \propto f_s \cos^2\theta_c),$$

where θ_c is the Cabbibo angle and f_s is the fraction of momentum carried by the s(or $\bar{s}$) quarks relative to that carried by the d quarks in the nucleon. In antineutrino interactions, however, the charm quark can only be produced by the process

$$\bar{\nu} + \bar{s} \to \mu^+ + \bar{c};\ (\sigma \propto f_s \cos^2\theta_c).$$

Therefore $\sigma^{\nu}(\mu^-\mu^+)/\sigma^{\bar{\nu}}(\mu^+\mu^-) \simeq 2$ provided that $f_s \simeq \tan^2\theta_c = 0.05$.

The X_{vis} and Y_{vis} distributions of the ν and $\bar{\nu}$ induced $\mu^-\mu^+$ events are shown in Figs. 15 and 16. The Y_{vis} distributions are similar for ν and $\bar{\nu}$ and are consistent with kinematic and acceptance cut-off in the low and high-y regions. The $\bar{\nu}$ induced dimuons, however, have a sharper X_{vis}

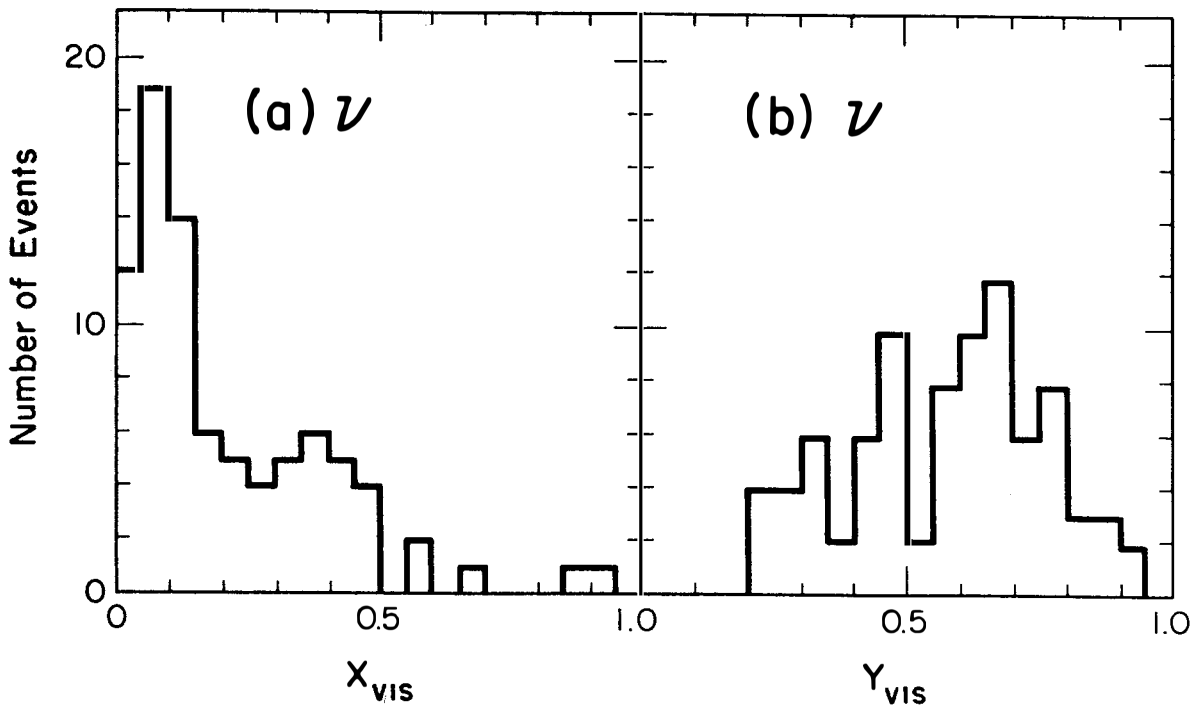

Fig.15 Distributions of X_{vis} and Y_{vis} for ν-induced $\mu^-\mu^+$ events.

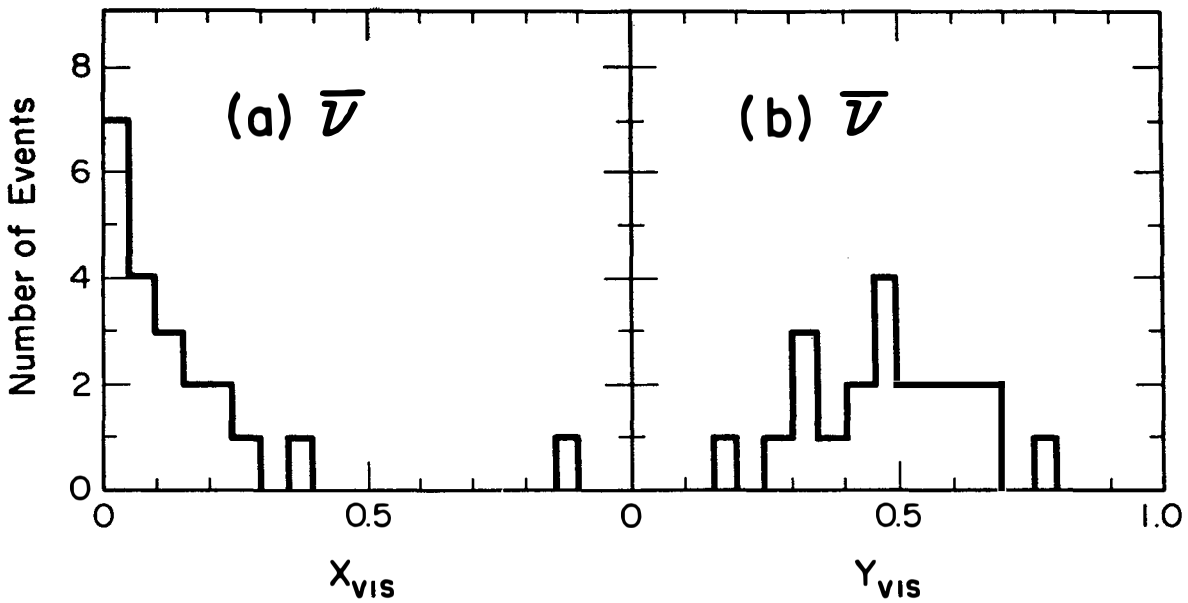

Fig.16 Distributions of X_{vis} and Y_{vis} for $\overline{\nu}$-induced $\mu^-\mu^+$ events.

distribution when compared to that of the ν data. This is also consistent with the GIM model since only the sea quark ($\bar{s}$) play the role for charm production by antineutrinos.

To give an overall perspective of the multimuon physics, we present in Table 3 the rates for neutrino induced $\mu^-\mu^+$, $\mu^-\mu^-$ and $\mu^-\mu^-\mu^+$, all relative to the charge-current interaction rate.

VI. Summary and Concluding Remarks

In summary, we have presented evidence for the production of prompt $\mu^-\mu^-$ events by neutrinos. The rate of the prompt $\mu^-\mu^-$ events relative to the prompt $\mu^-\mu^+$ rate is measured to be 0.10 ± 0.05 for $p_\mu > 5$ Gev/c, and 0.13 ± 0.05 for $p_\mu > 10$ Gev/c. The properties of the $\mu^-\mu^-$ events are similar to that of the $\mu^-\mu^+$ events. No clear evidence has as yet been established for prompt $\mu^+\mu^+$ events from $\bar{\nu}$ interactions.

What are the origins of the prompt $\mu^-\mu^-$ events? We remark that only $\mu^-\mu^+$ events are expected if charm particles are singly produced by neutrinos. Mechanisms to explain the $\mu^-\mu^-$ events which invokes new physics beyond charm must be measured against the following alternatives: (a) radiative or direct muon pair production in deep inelastic charged-current interactions;[10] (b) associated production of charmed particles.[11] Only trimuons can in principle be produced by mechanism (a). However, $\mu^-\mu^-$ events could result from this source if the μ^+ escapes experimental detection. Then one would expect $R(\mu^-\mu^-)/R(\mu^-\mu^-\mu^+) < 1$, contrary to the experimental observation (see Table 3). Therefore mechanism (a) is unlikely to be the dominant source for the $\mu^-\mu^-$ events. In associated charm production, both $\mu^-\mu^-$ and $\mu^-\mu^-\mu^+$ are expected. The ratio $R(\mu^-\mu^-)/R(\mu^-\mu^-\mu^+)$ should be about $\{BR(c \to \mu + x)\}^{-1} \sim 10$. The properties of the $\mu^-\mu^-$ events shown earlier are qualitatively compatible with the mechanism. The problem may lie in the absolute $\mu^-\mu^-$ rate.[11] If the measured $\mu^-\mu^-$ rate are confirmed with more data, then a large fraction, if not all, of the trimuons have to be attributed to associated charm production. More trimuon data is required to check consistency.

We have shown that both the rates and properties of the opposite-sign dimuon events are consistent with the GIM model. Based on this model, we may use the $\mu^-\mu^+$ data to determine f_s, the amount of strange quark relative to valence d-quark in the nucleon. The data gives approximately $f_s \sim \tan^2\theta_c = 0.05$.

	No E_ν cut††	E_ν > 100 GeV
$R(\mu^-\mu^+)/R(\mu^-)$	$(4.0 \pm 0.8) \times 10^{-3}$	$(6.5 \pm 1.3) \times 10^{-3}$
$R(\mu^-\mu^-)/R(\mu^-)$ †	$(4 \pm 2) \times 10^{-4}$	$(6.5 \pm 3.5) \times 10^{-4}$
$R(\mu^-\mu^-\mu^+)/R(\mu^-)$	$(9 \pm 5) \times 10^{-5}$	$(2.6 \pm 1.5) \times 10^{-4}$

TABLE 3. Multimuon rates relative to the rate of deep inelastic single muon events.

† Obtained using $R(\mu^-\mu^-)/R(\mu^-\mu^+) = 0.10 \pm 0.05$

††Averaged over the Quadrupole Triplet Spectrum

The data shown in this talk is the result of a collaboration of physicists from Fermilab, Harvard, Ohio State, Pennsylvania, Rutgers and Wisconsin. Individual members of the collaboration are A. Benvenuti, F. Bobisut, D. Cline, P. Cooper, M.G.D. Dilchriese, M. Heagy, R. Imlay, M. Johnson, T.Y. Ling, R. Lundy, A.K. Mann, P. McIntyre, S. Mori, D.D. Reeder, J. Rich, R. Stefanski and D. Winn.

References and Footnotes

*Work supported in part by the Dept. of Energy.

1. A Benvenuti et al., Phys. Rev. Lett. 34, 419 (1975).
2. J.D. Bjorken and S.L. Glashow, Phys. Lett. 11, 255 (1964); S.L. Glashow, J. Iliopoulous and L. Maiani, Phys. Rev. D2, 1285 (1970).
3. A. Benvenuti et al., Phys. Rev. Lett. 35, 1199 (1975), ibid 35, 1203 (1975).
4. B.C. Barish et al., Phys. Rev. Lett., 36, 939 (1976). M. Holder et al., Phys. Lett. 69B, 377 (1977).
5. B.C. Barish et al., Phys. Rev. Lett. 38, 577 (1977); A. Benvenuti et al., Phys. Rev. Lett 38, 1110 (1977) and 40,488 (1978).
6. A. Skuja, R. Stefanski and A. Windelbon, FNAL Technical Note TM469 (1974).
7. R. Stefanski and H.B. White, FNAL Technical Note TM26A (1976).
8. R. Imlay, Calculations of background from pion and kaon decays in neutrino interactions. (unpulbished)
9. M. Holder et al., Phys. Lett. 70B, 396 (1977).
10. J. Smith and J.A.M. Vermaseren, Stony Brook Report ITP-SB-77-66; R.M. Barnett et al., SLAC-PUB-2063 (1977); V. Barger, T. Gottschalk and R.J.N. Phillips, Wisconsin Report COO-881-9.
11. H. Goldberg, Phys. Rev. Lett. 39, 1598 (1977).